

## THE HIGH-ALBEDO KUIPER BELT OBJECT (55565) 2002 AW<sub>197</sub>

DALE P. CRUIKSHANK,<sup>1</sup> JOHN A. STANSBERRY,<sup>2</sup> JOSHUA P. EMERY,<sup>2,3</sup> YANGA R. FERNÁNDEZ,<sup>4</sup> MICHAEL W. WERNER,<sup>5</sup>  
DAVID E. TRILLING,<sup>2</sup> AND GEORGE H. RIEKE<sup>2</sup>

Received 2005 January 5; accepted 2005 March 23; published 2005 April 1

### ABSTRACT

We detected thermal emission from the Kuiper Belt object 2002 AW<sub>197</sub> in 2003 December and again in 2004 April using the Multiband Imaging Photometer on the *Spitzer Space Telescope*. In combination with the absolute visual magnitude, the thermal measurements indicate a geometric albedo of  $0.17 \pm 0.03$  and a diameter of  $700 \pm 50$  km. The albedo of 2002 AW<sub>197</sub> is significantly higher than the 0.04 value typically assumed for trans-Neptunian objects, and consequently the object is smaller than previously thought based on that assumption. Our thermal measurements at two wavelengths (24 and 70  $\mu\text{m}$ ) allow us to constrain the surface temperature and thereby place constraints on the thermal inertia. We find that the standard thermal model (STM) is inconsistent with the 24/70  $\mu\text{m}$  color unless we set the beaming parameter  $\eta > 0.95$ , indicating that the object has a significant thermal inertia and, therefore, that the STM is inappropriate. The other end-member thermal inertia model is the fast-rotator, or isothermal-latitude, model (ILM). The data are well represented by an ILM with the pole of rotation inclined to the Sun by  $45^\circ \pm 10^\circ$ . The high albedo is consistent with a surface containing significant amounts of weakly absorbing materials, with ices and/or fine-grained silicates as likely candidates.

*Subject headings:* infrared: solar system — Kuiper Belt — minor planets, asteroids

### 1. INTRODUCTION

We report here on the interpretation of measurements of the thermal flux of Kuiper Belt object (55565) 2002 AW<sub>197</sub> with the *Spitzer Space Telescope*. The dimensions of Kuiper Belt objects (KBOs) are generally estimated from their measured brightness in reflected sunlight at short wavelengths (0.4–0.9  $\mu\text{m}$ ) and an assumed albedo, but in a few cases measurements of the flux of emitted thermal radiation (together with the reflected flux) have permitted a direct determination of the size and albedo. The sizes and albedos of four KBOs have been estimated based on thermal measurements (Thomas et al. 2000; Jewitt et al. 2001; Lellouch et al. 2002; Altenhoff et al. 2004), including 2002 AW<sub>197</sub> (Margot et al. 2002), and the size of (50000) Quaoar was measured directly using the *Hubble Space Telescope* (Brown & Trujillo 2004). The calculation of the size and albedo of an object from the reflected and thermal fluxes is model-dependent, because several additional parameters must be measured or estimated (see below).

Kuiper Belt object 2002 AW<sub>197</sub> has an orbit with a semimajor axis of 47.50 AU, an eccentricity of 0.1274, and an inclination of 24:31. Its absolute magnitude is  $H = 3.27$ , and it does not have a strong light curve. Fornasier et al. (2004) reported *BVRI* photometry, and Doressoundiram et al. (2005) extended the photometry to the *JHK* bands. 2002 AW<sub>197</sub> is moderately red in the visible spectral region. The spectroscopic observations (1.42–2.46  $\mu\text{m}$ ) of Doressoundiram et al. (2005) showed no clear evidence of H<sub>2</sub>O ice absorption bands.

Shortly after the discovery of 2002 AW<sub>197</sub> by Brown et al. (2002), Margot et al. (2002) reported a  $4\sigma$  detection of the thermal emission at 1.2 mm wavelength, which, when com-

bined with a measurement of the reflected light, yielded a diameter of 886 (+115, –131 km), and *V*-band geometric albedo of 0.101 (+0.038, –0.022), more than twice the value of 0.04 usually assumed for primitive objects such as trans-Neptunian bodies.

### 2. NEW OBSERVATIONS AND DATA REDUCTION

We observed 2002 AW<sub>197</sub> with the *Spitzer Space Telescope* (Werner et al. 2004) using the Multiband Imaging Photometer for *Spitzer* (MIPS; Rieke et al. 2004) and the standard photometry template, with exposure times and details summarized in Table 1 (see Fig. 1). The photometry template includes dithers to provide a good point-spread function sampling and a better photometric performance in all three bands, and it provides a filled field of view for the 160  $\mu\text{m}$  band. The data were reduced, calibrated, and mosaicked using the MIPS instrument team analysis tools (Gordon et al. 2005). The most important difference from the standard pipeline processing is at 70  $\mu\text{m}$ , where an additional additive correction is derived from the data itself to remove artifacts due to latent images from the stimulator flashes.

### 3. PHOTOMETRY

Photometry was performed using circular apertures with diameters of 3", 15", and 24" at 24, 70, and 160  $\mu\text{m}$ , respectively. These small apertures (1.5 pixels radius in each band) maximize the signal-to-noise ratio (S/N) for faint sources and minimize the probability of photometric contamination by a background source. The background level and noise-equivalent flux density were estimated using approximately 10 apertures of the same size placed in the near vicinity of the source. This increased the S/N of our measurements by about 20% relative to photometry done using a comparable sky annulus centered at the target location. Results are given in Table 1. At 160  $\mu\text{m}$  we report the  $3\sigma$  upper limit for completeness; the value does not meaningfully constrain our thermal models. The absolute accuracies of the 24 and 70  $\mu\text{m}$  photometry are 10% and 20%, respectively. It is unlikely that

<sup>1</sup> NASA Ames Research Center, MS 245-6, Moffett Field, CA 94035-1000; dale.p.cruikshank@nasa.gov.

<sup>2</sup> Steward Observatory, University of Arizona, 933 North Cherry Avenue, Tucson, AZ 85721-0065.

<sup>3</sup> SETI Institute, 2035 Landings Drive, Mountain View, CA 94043.

<sup>4</sup> Institute for Astronomy, University of Hawaii, 2680 Woodlawn Drive, Honolulu, HI 96822.

<sup>5</sup> Jet Propulsion Laboratory, California Institute of Technology, 4800 Oak Grove Drive, Pasadena, CA 91109.

TABLE 1  
CIRCUMSTANCES OF THE OBSERVATIONS AND FLUXES

Wavelength Band ( $\mu\text{m}$ )	Date <sup>a</sup>	Exposure Time (s)	Heliocentric Distance $R$ (AU)	Geocentric Distance (AU)	Phase Angle (deg)	Flux (Error) <sup>b</sup> (mJy)
24	2003 Dec 1.0278	84	47.17	46.83	1.15	<0.18
70	2003 Dec 1.0326	400	...	...	...	16.2 (5.8)
160	2003 Dec 1.0410	100	...	...	...	<51
24	2004 Apr 13.1847	700	47.13	46.70	1.10	0.17 (0.02)
70	2004 Apr 13.1986	1000	...	...	...	13.4 (2.4)
160	2004 Apr 13.2111	80	...	...	...	<48

<sup>a</sup> On 2003 December 1, the *Spitzer*-centered coordinates (J2000) of the object were  $9^{\text{h}}03^{\text{m}}55^{\text{s}}.3$ ,  $+8^{\circ}43'04''0$ , and on 2004 April 4, the coordinates were  $9^{\text{h}}56^{\text{m}}29^{\text{s}}.4$ ,  $+9^{\circ}07'34''4$ .

<sup>b</sup> Errors shown are based solely on sky fluctuations in the images and do not include calibration uncertainties, which are 10% at 24  $\mu\text{m}$  and 20% at 70  $\mu\text{m}$ .

our 24 and 70  $\mu\text{m}$  photometry is contaminated significantly by emission from extragalactic sources. The areal density of  $0.1 \pm 0.05$  mJy 24  $\mu\text{m}$  sources (Papovich et al. 2004) is  $3 \text{ arcmin}^{-2}$ . For our aperture size ( $0.13 \text{ arcmin}^2$ ), this translates into a probability of 4% that our photometry could be contaminated by a 0.1 mJy source. The probability increases as fainter sources are considered, but only very slightly because the density of 24  $\mu\text{m}$  sources increases relatively slowly for flux densities less than 200  $\mu\text{Jy}$ . We compute the areal density of 70 and 160  $\mu\text{m}$  sources based on the results of Dole et al. (2004). At 70  $\mu\text{m}$  the density of sources brighter than  $\sim 3 \pm 1$  mJy is  $\sim 0.4 \text{ arcmin}^{-2}$ , which translates to a probability of a contaminating source in our  $0.19 \text{ arcmin}^2$  aperture of 8%. Unlike 24  $\mu\text{m}$ , at 70  $\mu\text{m}$  the density of sources decreases only slightly below about 10 mJy, so contamination by sources fainter than 3 mJy is likely; however, such faint sources would not affect our error bars appreciably. At 160  $\mu\text{m}$  2002 AW<sub>197</sub> is faint relative to the expected flux from background sources. The results of Dole et al. (2004) give the density of  $20 \pm 2$  mJy sources (comparable to both the flux we would predict for 2002 AW<sub>197</sub> and the measured fluctuations in our 160  $\mu\text{m}$  image) as  $0.2 \text{ arcmin}^{-2}$ ; the corresponding probability of a 20 mJy background source falling in our 160  $\mu\text{m}$  photometry aperture is then about 10%. Thus, a 20 mJy source at 160  $\mu\text{m}$  is significantly above the confusion limit and could in principle be detected by MIPS.

#### 4. THERMAL MODELS AND RESULTS

The standard thermal model (STM; Lebofsky & Spencer 1989) is the most widely used model for interpreting observations of thermal emission from small bodies in the asteroid main belt and the outer solar system (see Tedesco et al. 2002;

Fernández et al. 2002; Campins et al. 1994). The model assumes a spherical body whose surface is in instantaneous equilibrium with the insolation, equivalent to assuming either a thermal inertia of zero, a nonrotating body, or a rotating body illuminated and viewed pole-on. In the STM the subsolar point temperature is

$$T_0 = [S_0(1 - p_v q)/(\eta \epsilon \sigma)]^{1/4}, \quad (1)$$

where  $S_0$  is the solar constant at the distance of the body,  $p_v$  is the geometric albedo,  $q$  is the phase integral (assumed here to be 0.36),  $\eta$  is the beaming parameter,  $\epsilon$  is the emissivity (which we set to 0.9), and  $\sigma$  is the Stefan-Boltzmann constant. Given  $T_0$ , the temperature as a function of position on the surface is  $T = T_0 \mu^{1/4}$ , where  $\mu$  is the cosine of the insolation angle. The nightside temperature is zero. Surface roughness leads to localized variations in surface temperature and non-isotropic thermal emission (beaming) because individual points on the surface radiate their heat preferentially in the sunward direction, rather than isotropically. Thus, when viewed at small phase angles, rough surfaces are warmer than smooth ones, and the thermal emission tends to be dominated by emission from the warmer patches. This effect is captured by the beaming parameter,  $\eta$ . Lebofsky et al. (1986) found  $\eta = 0.76$  for Ceres and Vesta; the nominal range for  $\eta$  is 0–1, with unity corresponding to a perfectly smooth surface (Lebofsky & Spencer 1989). In modeling the thermal emission from a large sample of Jovian Trojan asteroids, Fernández et al. (2003) found a typical value of  $\eta$  for that population of about 0.94, which we adopt here as likely to be appropriate for outer solar system minor planets.

The thermal emission from a target is calculated by computing a surface integral of the Planck function over the visible portion of the object. The Planck function at a particular point on the surface depends on the calculated temperatures (eq. [1]) and the wavelength of interest. This flux density is then scaled by a dilution factor proportional to  $D^2 \Phi / \Delta^2$ , where  $D$  is the diameter,  $\Phi$  is a factor to account for the nonzero phase angle of observation, and  $\Delta$  is the geocentric distance. For KBOs observed at very small phase angles, the correction factor (empirically determined to be  $0.01 \text{ mag deg}^{-1}$  in the mid-infrared; Lebofsky & Spencer 1989) gives a value of  $\Phi$  near unity and introduces negligible uncertainty. The total flux density thus depends on both the target's unknown diameter,  $D$ , and albedo,  $p_v$ , as well as its distance from the Sun and the observer. Solutions for the size and albedo require a second equation; the object's visible magnitude typically provides this constraint. We used the absolute visual magnitude,  $H_V = 3.27$ , to relate

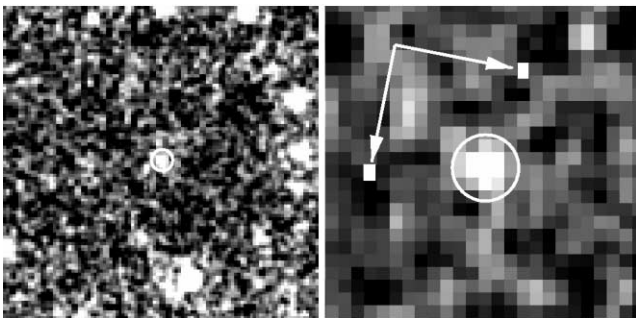


FIG. 1.—MIPS images of 2002 AW<sub>197</sub> at 24  $\mu\text{m}$  (left) and 70  $\mu\text{m}$  (right). Each image is  $2'$  on a side. Arrows indicate the image orientation relative to J2000 coordinates. White circles are centered at the predicted coordinates at the epoch of the observations, and their sizes indicate the approximate sizes of the *Spitzer* beam at the two wavelengths.

the diameter and albedo via  $D = 10^{-H_V/5} 1329/p_V^{1/2}$  (e.g., Harris 1998), where  $D$  is the diameter in units of kilometers.

The 24 and 70  $\mu\text{m}$  photometry and a series of best-fitting models are shown in Figure 2. Using the values of  $q$  and  $\epsilon$  noted above, we allowed  $\eta$  to vary. The best fit to the data in Figure 2a has  $\eta = 1.2$ , with  $D = 694$  km and  $p_V = 0.18$ . It is not unusual to allow  $\eta$  to range above unity (Harris 1998; Fernández et al. 2003; Delbo et al. 2003) when fitting thermal data with the STM. As can be seen from equation (1),  $\eta > 1$  will result in overall lower surface temperatures, even though  $\eta$  was traditionally introduced to model elevated localized temperatures (as viewed at small phase) caused by roughness. We interpret  $\eta > 1$  to be an indication that the body has a nonzero thermal inertia and a relatively short rotation period, and therefore that the idealized assumptions in the STM do not perfectly apply. As discussed below, it is not particularly surprising that 2002 AW<sub>197</sub> departs from the STM prediction.

The isothermal latitude model (ILM) is the opposing end-member model to the STM: the target is assumed to have a surface with infinite thermal inertia or, equivalently, to rotate instantaneously (also called the “fast-rotator model”; Lebofsky & Spencer 1989). In real terms, the ILM applies for objects with rotation periods much shorter than the timescale for radiative cooling of the surface. It is also typically assumed that the subsolar latitude is zero, although other geometries can be readily computed. Strictly speaking, under the ILM  $\eta = 1$ . Two ILM models that fit the data are also shown in Figure 2b. We were unable to fit the data under the assumption that  $\eta = 1$ , and so we again allowed it to be a free parameter. The resulting fit has  $\eta = 0.43$ , giving  $D = 658$  km and  $p_V = 0.20$ . We interpret  $\eta < 1$  under the ILM as an indication that the thermal inertia could actually be rather low (although the STM results indicate that it is very likely greater than zero). An alternative ILM fit can be achieved by allowing the position of the rotation axis to vary, such that the subsolar (and subobserver) latitude changes. In the limit that the subsolar latitude is set to  $90^\circ$ , the ILM is equivalent to the STM. We fit the ILM to our data, allowing the subsolar latitude to be a free parameter and setting  $\eta = 1$ . The resulting fit has a subsolar latitude of  $45^\circ$ , giving  $D = 725$  km and  $p_V = 0.17$ .

We have additionally fit our photometry with a thermophysical model (see Spencer 1990), which includes the effects of surface roughness ( $\theta$ ) and finite thermal inertia ( $\Gamma$ ). (The units of  $\Gamma$  are  $\text{J m}^{-2} \text{K}^{-1} \text{s}^{-1/2}$ ; in these units Pluto’s thermal inertia, as measured by the *Infrared Space Observatory* [Lellouch et al. 2000], is 15–100, whereas the Moon’s is 50.) For these models we assumed a subsolar latitude of  $0^\circ$  and considered rotation periods of  $P = 10$  hr (consistent with KBO periods) and  $P = 154$  hr (Pluto’s period). Fits with a smooth surface and  $P = 10$  hr yield  $\Gamma = 0.45$ ,  $D = 698$  km, and  $p_V = 0.18$ . In this scheme, increasing surface roughness will increase the thermal inertia of the model that best fits the data. Increasing  $P$  will have the same effect. Using extremes of surface roughness ( $\theta = 67^\circ$ ) and rotation ( $P = 154$  hr) yields  $\Gamma = 8.7$ ,  $D = 686$  km, and  $p_V = 0.18$ . As illustrated in the preceding section, a larger thermal inertia would apply for non-zero subsolar latitude models; nevertheless, it is very likely that the value for 2002 AW<sub>197</sub> is well below 20.

As a self-consistency check, we note that these derived values for  $\Gamma$  imply that we would expect 2002 AW<sub>197</sub> to have thermal behavior intermediate between the STM and ILM, as shown above. Spencer et al. (1989) introduced a thermophysical parameter  $\Theta$  to quantify the tendency of an object toward one extreme thermal behavior or the other. The quantity is given

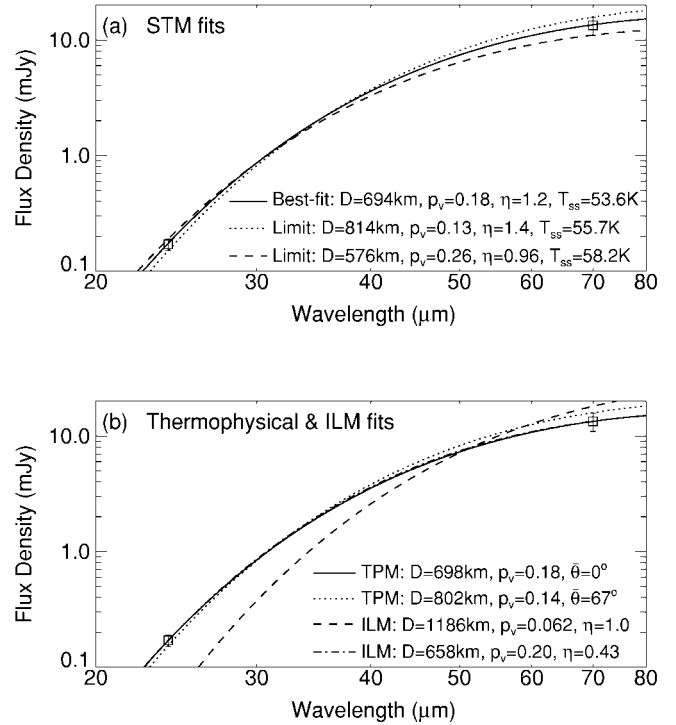


FIG. 2.—(a) STM fits to the *Spitzer* 24 and 70  $\mu\text{m}$  data from Table 1.  $T_{ss}$  is the temperature of the subsolar point calculated in a given model. (b) Thermophysical model (TPM) and ILM fits to the data in Table 1. For the ILM with  $p_V = 0.062$ ,  $T_{ss} = 44.0$  K; for  $p_V = 0.20$ ,  $T_{ss} = 53.7$  K. The best-fit TPM (solid line) has a thermal inertia ( $\Gamma$ ) of  $0.45 \text{ J m}^{-2} \text{K}^{-1} \text{s}^{-1/2}$ , a maximum temperature of  $55.9$  K, and a 10 hr rotation period. The TPM fit to the extremes of the error bars (dotted line) has  $\Gamma = 8.7 \text{ J m}^{-2} \text{K}^{-1} \text{s}^{-1/2}$ , a maximum temperature of  $53.9$  K, and a 154 hr rotation period.

by  $\Theta = \Gamma \sqrt{\omega} / (\epsilon \sigma T_{ss}^3)$ , where  $\omega = 2\pi/P$  and  $T_{ss}$  is the subsolar temperature. Bodies that perfectly obey the STM or ILM would have  $\Theta \rightarrow 0$  or  $\infty$ , respectively. We calculate that 2002 AW<sub>197</sub> has  $\Theta = 0.7$ , placing it in the border regime between the two models. Such a low but nonzero thermal inertia implies either a very porous surface or perhaps the presence of a material that has a low intrinsic thermal inertia (e.g., amorphous  $\text{H}_2\text{O}$  ice).

From these STM, ILM, and thermophysical model fits to the data, as well as from explorations of the range of parameters that provide thermal models that are consistent with the errors on our measurements, we find that the diameter of 2002 AW<sub>197</sub> is likely  $620 \text{ km} < D < 775 \text{ km}$  and that the visible geometric albedo is  $0.14 < p_V < 0.23$ . These ranges exclude some of the most extreme models that fit the data but span most of the reasonable models, and they can be treated as a  $\pm 1 \sigma$  range. Including only the results from the *best-fit models*, and assuming that the differences between them dominate the systematic uncertainties, we conclude that  $650 \text{ km} < D < 750 \text{ km}$  and  $0.14 < p_V < 0.20$ .

## 5. DISCUSSION AND CONCLUSIONS

Both our measurements and those of Margot et al. (2002) agree that the albedo of 2002 AW<sub>197</sub> is much larger than the value of 0.04 commonly assumed for KBOs, and our data indicate that this object is somewhat smaller and has an even higher albedo than was found by Margot et al. (2002) based on their 1.2 mm data. We have used our model fits to the *Spitzer* data to predict the 1.2 mm flux we would expect,

assuming that emissivity is constant with wavelength. The mean and standard deviation of the predicted 1.2 mm fluxes, corrected to the epoch of the Margot et al. observations (2002 April 15; J. L. Margot 2004, private communication) are  $F_{1.2\text{ mm}} = 0.60 \pm 0.13$  mJy. The maximum 1.2 mm flux predicted by our models is 0.76 mJy, just consistent with the  $1\sigma$  lower limit of the measured 1.2 mm flux, while the 1.2 mm prediction is  $1.5\sigma$  below the measurement. Likewise, our  $1\sigma$  results for albedo and diameter ( $p_V = 0.14$ ,  $D = 750$  km) are consistent with the  $1\sigma$  values from Margot et al. ( $p_V = 0.14$ ,  $D = 755$  km). Thus, the nominal values from the two independent sets of observations are about  $2\sigma$  apart. In the absence of a strong visible light curve, it seems unlikely that a difference in subobserver longitudes can reconcile the discrepancy. The emissivity for some main-belt asteroids is wavelength-dependent in the far-IR (Müller & Lagerros 1998, 2002). However, the trend is for emissivity to decline with wavelength, which would actually

amplify the discrepancy between the *Spitzer* and submillimeter results. At this time we have not found a way to reconcile the two answers. Our  $70\ \mu\text{m}$  flux measurements in 2003 December and 2004 April are consistent, as are the  $24\ \mu\text{m}$  limit and detection for those two epochs.

This albedo is significantly higher than the albedos estimated or measured for all other Kuiper Belt objects. It is the highest for an object that was actually measured at thermal wavelengths, although estimates of high albedos have been made for objects for which upper limits to thermal fluxes have been determined from observations at millimeter wavelengths (Altenhoff et al. 2004).

This work is based in part on observations made with the *Spitzer Space Telescope*, operated by JPL/Caltech under NASA contract 1407. Support for this work was provided by NASA through contract 960785, issued by JPL/Caltech. We thank Martin Harwit for his helpful comments.

#### REFERENCES

- Altenhoff, W. J., Bertoldi, F., & Menten, K. M. 2004, *A&A*, 415, 771  
 Brown, M. E., & Trujillo, C. A. 2004, *AJ*, 127, 2413  
 Brown, M. E., Trujillo, C. A., Helin, E. F., Pravdo, S., Lawrence, K., Hicks, M., & Marsden, B. G. 2002, *MPE Circ.* 2002-O30  
 Campins, H., Telesco, C. M., Osip, D. J., Rieke, G. H., Rieke, M. J., & Schulz, B. 1994, *AJ*, 108, 2318  
 Delbo, M., Harris, A. W., Binzel, R. P., Pravec, P., & Davies, J. K. 2003, *Icarus*, 166, 116  
 Dole, H., et al. 2004, *ApJS*, 154, 87  
 Doressoundiram, A., et al. 2005, *A&A*, in press  
 Fernández, Y. J., Jewitt, D. C., & Sheppard, S. S. 2002, *AJ*, 123, 1050  
 Fernández, Y. J., Sheppard, S. S., & Jewitt, D. C. 2003, *AJ*, 126, 1563  
 Fornasier, S., Dotto, E., Barucci, M. A., & Barbieri, C. 2004, *A&A*, 422, L43  
 Gordon, K. D., et al. 2005, *PASP*, in press  
 Harris, A. W. 1998, *Icarus*, 131, 291  
 Jewitt, D., Aussen, H., & Evans, A. 2001, *Nature*, 411, 446  
 Lebofsky, L. A., & Spencer, J. R. 1989, in *Asteroids II*, ed. R. P. Binzel, T. Gehrels, & M. S. Matthews (Tucson: Univ. Arizona Press), 128  
 Lebofsky, L. A., et al. 1986, *Icarus*, 68, 239  
 Lellouch, E., Laureijs, R., Schmitt, B., Quirico, E., de Bergh, C., Crovisier, J., & Coustenis, A. 2000, *Icarus*, 147, 220  
 Lellouch, E., Moreno, R., Ortiz, J. L., Paubert, G., Doressoundiram, A., & Peixinho, N. 2002, *A&A*, 391, 1133  
 Margot, J. L., Trujillo, C., Brown, M. E., & Bertoldi, F. 2002, *BAAS*, 34, 871  
 Müller, T. G., & Lagerros, J. S. V. 1998, *A&A*, 338, 340  
 ———. 2002, *A&A*, 381, 324  
 Papovich, C., et al. 2004, *ApJS*, 154, 70  
 Rieke, G. H., et al. 2004, *ApJS*, 154, 25  
 Spencer, J. R. 1990, *Icarus*, 83, 27  
 Spencer, J. R., Lebofsky, L. A., & Sykes, M. V. 1989, *Icarus*, 78, 337  
 Tedesco, E. F., Noah, P. V., Noah, M., & Price, S. D. 2002, *AJ*, 123, 1056  
 Thomas, N., et al. 2000, *ApJ*, 534, 446  
 Werner, M. W., et al. 2004, *ApJS*, 154, 1